Inorg. Chem. **2005**, *44*, 5322–5327

Negative Magnetoresistance in a Magnetic Semiconducting Zintl Phase: $Eu_3In_2P_4$

Jiong Jiang, Marilyn M. Olmstead, and Susan M. Kauzlarich*

Department of Chemistry, One Shields Ave., University of California, Davis, California 95616

Han-Oh Lee, Peter Klavins, and Zachary Fisk

Department of Physics, One Shields Ave., University of California, Davis, California 95616

Received March 17, 2005

A new rare earth metal Zintl phase, $Eu_3In_2P_4$, was synthesized by utilizing a metal flux method. The compound crystallizes in the orthorhombic space group *Pnnm* with the cell parameters $a = 16.097(3)$ Å, $b = 6.6992(13)$ Å, $c = 4.2712(9)$ Å, and $Z = 2$ ($T = 90(2)$ K, R1 = 0.0159, wR2 = 0.0418 for all data). It is isostructural to $Sr_3In_2P_4$. The structure consists of tetrahedral dimers, $[In_2P_2P_{4/2}]^{6-}$, that form a one-dimensional chain along the *c* axis. Three europium atoms interact via a Eu–Eu distance of 3.7401(6) Å to form a straight line triplet. Single-crystal magnetic measurements show anisotropy at 30 K and a magnetic transition at 14.5 K. High-temperature data give a positive Weiss constant, which suggests ferromagnetism, while the shape of susceptibility curves (χ vs *T*) suggests antiferromagnetism. Heat capacity shows a magnetic transition at 14.5 K that is suppressed with field. This compound is a semiconductor according to the temperature-dependent resistivity measurements with a room-temperature resistivity of 0.005(1) Ω m and $E_g = 0.452(4)$ eV. It shows negative magnetoresistance below the magnetic ordering temperature. The maximum magnetoresistance ($\Delta\rho/\rho(H)$) is 30% at 2 K with $H = 5$ T.

Introduction

Zintl phases have been extensively studied since the Zintl concept was first presented. In this class of compounds, electropositive elements (alkali and alkaline earth metals) donate electrons to electronegative group 13−16 elements, and the compound is valence precise.[1,2] In recent years, the Zintl boundary has been extended to rare earth metal containing compounds. This approach has led to the discovery of many complex new structures.[3,4] In addition, because of the unique electron configuration of rare earth metals, rare earth metal Zintl phases were found to have special physical properties. Thermoelectricity[5,6] and superconductivity[7] have both been discovered in rare earth metal Zintl phases. Rare earth metal Zintl phases containing Eu and Yb are most interesting, because of the possibility of variable valence states and localized magnetic moment. Eu^{2+} has seven unpaired f electrons. There are several Eu-containing Zintl phases that show unusual magnetic and magnetotransport properties.[8−13] Eu-containing Zintl phases are typically antiferromagetic with a low magnetic ordering temperature,[14,15] but many of them show a positive Weiss constant, which suggests a ferromagnetic correlation in the paramagnetic region.[11,12,16]

* Corresponding author. E-mail: smkauzlarich@ucdavis.edu.

(1) Kauzlarich, S. M., *Chemistry, Structure, and Bonding of Zintl Phases and Ions*. VCH Publishers: New York, 1996; p 306.
(2) Schäfer, H.; Eisenmann, B.; Müller, W. *Angew. Chem., Int. Ed. Engl.* **1973**, *12*, 694−712.
(3) Mills, A. M.; Lam, R.; Ferguson, M. J.; Deakin, L.; Mar, A. *Coord. Chem. Rev.* **2002**, *233*−*234*, 207−222.
(4) Gascoin, F.; Sevov, S. C. *Inorg. Chem.* **2003**, *42*, 8567−8571.
(5) Mahan, G.; Sales, B.; Sharp, J. *Phys. Today* **1997**, March, 42.
(6) Kim, S.-J.; Ireland, J. R.; Kannewurf, C.; Kanatzidis, M. G. *J. Solid State Chem.* **2000**, *155*, 55−61.
(7) Mills, A. M.; Deakin, L.; Mar, A. *Chem. Mater.* **2001**, *13*, 1778−1788.
(8) Kauzlarich, S. M.; Payne, A. C.; Webb, D. J. Magnetism and Magnetotransport Properties of Transition Metal Zintl Isotypes. In *Magnetism: Molecules to Materials III*; Miller, J. S., Drillon, M., Eds. Wiley-VCH: Weinham, 2002; pp 37−62.
(9) Chan, J. Y.; Kauzlarich, S. M.; Klavins, P.; Liu, J.-Z.; Shelton, R. N.; Webb, D. J. *Phys. Rev. B: Condens. Matter* **2000**, *61*, 459−463.
(10) Payne, A. C.; Olmstead, M. M.; Kauzlarich, S. M.; Webb, D. J. *Chem. Mater.* **2001**, *13*, 1398−1406.
(11) Payne, A. C.; Sprauve, A. E.; Holm, A. P.; Olmstead, M. M.; Kauzlarich, S. M.; Klavins, P. *J. Alloys Compd.* **2002**, *338*, 229−234.
(12) Payne, A. C.; Sprauve, A. E.; Olmstead, M. M.; Kauzlarich, S. M.; Chan, J. Y.; Reisner, B. A.; Lynn, J. W. *J. Solid State Chem.* **2002**, *163*, 498−505.
(13) Badding, J. V.; Stacy, A. M. *Phys. Rev. B: Condens. Matter* **1987**, *35*, 8880−3.

10.1021/ic0504036 CCC: $30.25
Published on Web 06/24/2005

In the last several years the $Ln_{14}MnPn_{11}$ system has been explored,[8−10,17,18] where Ln = Eu, Yb, Pn = P, Sb, As, because of the unique magnetic and electronic properties found in this system. In an effort to make large crystals of $Eu_{14}MnP_{11}$[10] utilizing a metal In flux, Eu_3InP_3 was discovered.[19] The structure of Eu_3InP_3 can be explained by the Zintl concept and is a semiconductor. The valence of Eu was determined by Mössbauer spectroscopy to have a value of 2+. There are three crystallographically different Eu^{2+} sites. The three sites magnetically interact with each other, which results in several magnetic ordering transitions below 14.5 K.

In this paper, we introduce a new Eu-containing Zintl compound, $Eu_3In_2P_4$. The compound is isostructural with the main group Zintl phases $Sr_3In_2P_4$ and $Ca_3In_2As_4$.[20] Magnetic measurements of this compound show features of both ferromagnetism and antiferromagnetism. At low temperatures, $Eu_3In_2P_4$ shows magnetoresistance.

Experimental Section

Synthesis. The starting materials were $^1/_8$" Eu ribbon (99.999%, Ames Lab), cut into small pieces, red P (J. Matthey, Puratronic), crushed into small pieces, and In shot (Aesar, 99.99%), used as received. All reactants were mixed in a mole ratio of Eu:In:P = 3:120:4 under N_2 atmosphere. The elements were placed in a 2 mL cylindrical alumina crucible with the Eu (136.8 mg) and P (37.2 mg) between two layers of In (4.1335 g). Another crucible filled with quartz wool was inverted and covered the reaction crucible, and the entire system was sealed in a quartz ampule under $^1/_5$ atm Ar. The sealed reaction container was heated accordingly: ramp to 500 °C over a period of 1 h and dwell for 1 h and ramp to 1100 °C over a period 1 h, dwell for 6 h, cool at 3 °C/h to 850 °C, and dwell for 15 h. The reaction vessel was removed from the furnace at 850 °C, inverted, and centrifuged. Large, 1−2 mm^3, crystals were obtained. When exposed to air, the black crystals decompose into a yellow powder. Therefore, the reaction product was kept in a N_2-filled drybox equipped with a microscope and protected from air exposure for all subsequent measurements.

Single-Crystal X-ray Diffraction. The compound structure was determined by single-crystal X-ray diffraction. The air-sensitive crystal was stored in Exxon Paratone-N oil when taken out of the drybox. To obtain a crystal of suitable size, a large crystal was cut with a stainless steel blade into $0.14 \times 0.12 \times 0.09$ mm^3. The crystal was mounted on the tip of a quartz fiber and positioned under a 90(2) K cold N_2 stream provided by a CRYO Industries low-temperature apparatus on the goniometer head of a Bruker SMART 1000 diffractometer. Diffraction data were collected using graphite-monochromated Mo Kα radiation. An absorption correction was applied using the program SADABS v2.10. The structure was solved and refined with the aid of the SHELXTL 6.10 program package.[21] Direct methods were used in solving the structure. The final refinement gave R1 = 0.0159 and wR2 = 0.0418, with the largest difference in the Fourier map being 1.107 e $Å^{-3}$, 0.87 Å from Eu(2). Some details of the crystallography and refinement parameters are listed in Table 1.

Table 1. Selected Crystallographic Crystal Data

empirical formula	$Eu_3In_2P_4$
formula weight	809.40
temperature	90(2) K
wavelength	0.710 73 Å
crystal system	orthorhombic
space group	Pnnm
unit cell dimensions	$a = 16.097(3)$ Å $b = 6.6992(13)$ Å $c = 4.2712(9)$ Å
volume	460.58(16) $Å^3$
Z	2
density (calcd)	5.836 g/cm^3
absorption coefficient	25.663 mm^{-1}
$F(000)$	694
crystal size	$0.14 \times 0.12 \times 0.09$ mm^3
θ range for data collection	2.53°−28.26°
index ranges	$-21 \le h \le 21$, $-8 \le k \le 8$, $-5 \le l \le 5$
reflections collected	4995
independent reflections	646 [R(int) = 0.0273]
completeness to $\theta = 28.26°$	99.8%
refinement method	full-matrix least-squares on F^2
data/restraints/parameters	646/0/30
goodness-of-fit on F^2	2.179
final R indices [$I > 2\sigma(I)$]	R1[a] = 0.0159, wR2[b] = 0.0418
R indices (all data)	R1 = 0.0159, wR2 = 0.0418
extinction coefficient	0.0181(5)
largest diff peak and hole	1.107 and −1.512 e $Å^{-3}$

[a] $R1 = \sum||F_o| - |F_c||/\sum|F_o|$. [b] $wR2 = [\sum[w(F_o^2 - F_c^2)^2]/\sum[w(F_o^2)^2]]^{1/2}$.

X-ray Powder Diffraction. The crystals were ground to a fine powder with an agate mortar and pestle in a N_2 atmosphere drybox and then mixed with approximately 15% silicon standard and placed between two pieces of cellophane tape. The sample was transferred to a Guinier camera (Cu Kα1) with a vacuum sample chamber. The diffraction pattern was compared with the calculated diffraction pattern obtained from the single-crystal refinement using the computer program Crystaldiffract 3.2. The powder diffraction pattern could be indexed according to the single-crystal structure. There were no unindexed diffraction lines.

Magnetic Susceptibility Measurement. The magnetic measurements were obtained using a Quantum Design MPMS superconducting quantum interference device (SQUID) magnetometer. A 2.01 mg single crystal was used for the measurements. The crystal was protected in Paratone oil and fixed inside a drinking straw, which was used as a sample holder. The *a*, *b*, and *c* axis orientations were determined by single-crystal diffraction, so the magnetic properties in directions parallel to *a*, *b*, and *c* axis could be measured. Zero-field-cooling (ZFC) and field-cooling (FC) measurements were performed between 2 and 300 K with applied fields of 0.01, 0.1, and 5 T. Magnetization curves were also measured between −2 and 2 T at 5 K. The data were reproduced on several different crystals.

Charge-Transport Measurement. Resistivity of $Eu_3In_2P_4$ was measured on a crystal of $0.6 \times 0.5 \times 0.3$ mm^3 dimensions. Platinum

(14) Chan, J. Y.; Rehr, A.; Webb, D. J.; Kauzlarich, S. M. *Chem. Mater.* **1997**, *9*, 2131−2138.
(15) Ernet, U.; Muellmann, R.; Mosel, B. D.; Eckert, H.; Poettgen, R.; Kotzyba, G. *J. Mater. Chem.* **1997**, *7*, 255−257.
(16) Bobev, S.; Bauer, E. D.; Thompson, J. D.; Sarrao, J. L. *J. Magn. Magn. Mater.* **2004**, *277*, 236−243.
(17) Fisher, I. R.; Wiener, T. A.; Bud′ko, S. L.; Canfield, P. C.; Chan, J. Y.; Kauzlarich, S. M. *Phys. Rev. B: Condens. Matter* **1999**, *59*, 13829−13834.
(18) Holm, A. P.; Kauzlarich, S. M.; Morton, S. A.; Waddill, G. D.; Pickett, W. E.; Tobin, J. G. *J. Am. Chem. Soc.* **2002**, *124*, 9894−9898.
(19) Jiang, J.; Payne, A. C.; Olmstead, M. M.; Lee, H.-o.; Klavins, P.; Fisk, Z.; Kauzlarich, S. M.; Hermann, R. P.; Grandjean, F.; Long, G. J. *Inorg. Chem.* **2005**, *44*, 2189−2197.
(20) Cordier, G.; Schäfer, H.; Stelter, M. *Z. Naturforsch.* **1986**, *41b*, 1416−1419.
(21) Sheldrick, G. M. *SHELXTL*, 6.10 ed.; Bruker Analytical X-ray Instruments, Inc.: Madison, WI, 1997.

wires were attached to the crystal with Epo-Tek silver epoxy. The temperature-dependent resistivity of this compound was measured by both two-lead and four-lead methods because of the measurement limits. A four-lead method was employed from 300 to 130 K. A constant current of 100 nA was applied through two outer leads with a Keithley Model 224 current source, and a Keithley 181 voltmeter was used to measure voltage between the two inner leads. Below 130 K, the resistance became too high to measure with the voltmeter (200 mV), and a two-lead method was used. A Keithley Model 617 programmable electrometer that can measure up to 200 GΩ was employed for the two-lead method. Resistance as a function of temperature was measured in both 0 and 3 T applied fields.

Heat Capacity Measurement. Heat capacity of $Eu_3In_2P_4$ was measured with a Quantum Design Physical Property Measurement System (PPMS) in the temperature range from 1.8 to 30 K. The measurement was performed with applied fields of 0 and 1 T using a thermal relaxation method. A crystal of 1.93 mg was used for the measurement. The sample was mounted on the sample holder with Apiezon N-grease. There is a possibility of exposure of the sample to air for less than 30 s when putting the sample into the PPMS. Addenda measurements were done prior to sample measurements. Entropy was calculated by integrating the specific heat divided by temperature in the measured temperature range. Large crystals of the nonmagnetic analogue, $Sr_3In_2P_4$, were not available in order to subtract the nonmagnetic contributions to the C_p. However, the electronic and phonon contributions to the heat capacity are expected to be small compared to the magnetic contribution at low temperatures in this semiconductor.

Results and Discussion

Synthesis. Large high purity crystals can be grown from flux reactions.[22,23] In the synthesis of this compound, indium was used as a flux because of its low melting point, inertness to the alumina crucible, small wetting effect, and low vapor pressure. The appearance of $Eu_3In_2P_4$ is very similar to that of Eu_3InP_3 and was initially discovered as a side product in the flux synthesis of Eu_3InP_3. Both are black needle-shaped crystals. The flux composition was varied until $Eu_3In_2P_4$ could be produced as the sole product. The synthetic conditions for these two compounds are similar, except that the reactants of $Eu_3In_2P_4$ have a higher P:Eu ratio. $Eu_3In_2P_4$ could not be prepared from stoichiometric amounts of the elements in a sealed tantalum ampule heated at 1100 °C for 5 days. Instead, Eu_3InP_3 is obtained as the main product. It is possible that part of the In or P reacted with the tantalum tube, causing the reaction to be off-stoichiometry. We did not attempt further experiments varying temperature or stoichiometry for tantalum tube reactions, since the product could be obtained in high yield from the flux reaction.

Structure. A study of two main group Zintl phases of the 3−2−4 structure, $Sr_3In_2P_4$ and $Ca_3In_2As_4$,[20] was published in 1986. The structure type is orthorhombic with space group P*nnm*. $Eu_3In_2P_4$ is the first magnetic compound of this structure type. Table 1 provides the X-ray data collection

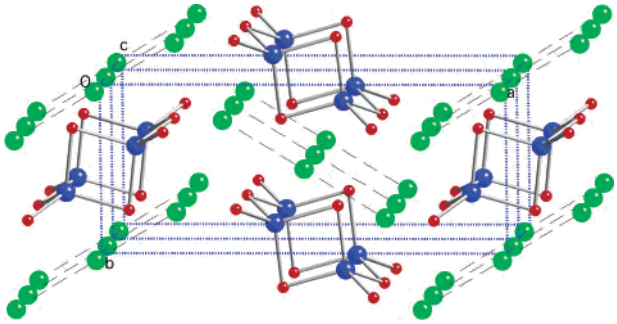

Figure 1. Crystal structure of $Eu_3In_2P_4$. Eu, In, and P atoms are indicated as green, blue, and red balls, respectively. The dotted lines represent the closest Eu−Eu distances.

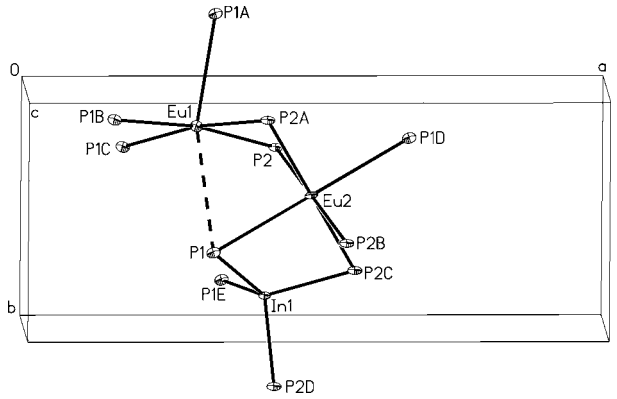

Figure 2. A partial structure of $Eu_3In_2P_4$ showing the numbering scheme and the local europium and indium environments. The anisotropic displacement ellipsoids are shown at the 90% probability level.

parameters and the structure solution and refinement results. There are two crystallographically unique Eu and P sites in this compound.

The crystal structure of $Eu_3In_2P_4$ is shown in Figure 1. The compound is composed of units of two edge-shared tetrahedra, $[In_2P_4]^{6-}$, that are corner shared and stacked to form a chain along the *c* axis. Eu atoms surround the chains. Figure 2 shows the local environments of Eu(1), Eu(2), and In. In−P distances range from 2.5618(16) to 2.6369(10) Å and the P−In−P angles are from 99.42(4)° to 113.16(4)°, almost identical to those of $Sr_3In_2P_4$.[20] The longer In−P distances come from corner-shared phosphorus (P1). There are six P atoms around each Eu atom forming distorted octahedra. The Eu−P distances are also very similar to the Sr−P distances in $Sr_3In_2P_4$. The Eu−P distances are between 2.9599(11) and 3.1905(16) Å, except the 3.5827(17) Å Eu(1)−P(1) (shown as a dash line in Figure 2). The distance range is typical for Eu−P binaries, such as EuP_7, Eu_3P_4, and EuP.[24] With such distances, Eu and P generally show covalent interactions.[24] The Eu-only lattice is very interesting in this compound. Eu(2) occupies a site with 2/m symmetry, while Eu(1) resides on the mirror plane. By symmetry, two Eu(1) atoms build a Eu(1)−Eu(2)−Eu(1) straight line triplet with each Eu(2) atom, as indicated with the dotted line in Figure 1. These triplets are in the *ab* plane. The Eu(1)−Eu(2) distance in a triplet is 3.7401(6) Å. This is the shortest

(22) Fisk, Z.; Remeika, J. P., Growth of Single Crystals from Molten Metal Fluxes. In *Handbook on the Physics and Chemistry of Rare Earths*, Gschneidner, K. A., Eyring, L., Eds.; Elsevier Science Publishers B. V.: Amsterdam, 1989; Vol. 12, p 53.
(23) Canfield, P. C.; Fisk, Z. *Philos. Mag. B* **1992**, *65*, 1117.
(24) Hulliger, F. Rare Earth Pnictides. In *Handbook on the Physics and Chemistry of Rare Earths*; Gschneidner, K. A. J., Eyring, L. R., Eds.; North-Holland: Amsterdam, 1979; Vol. 4, pp 153−236.

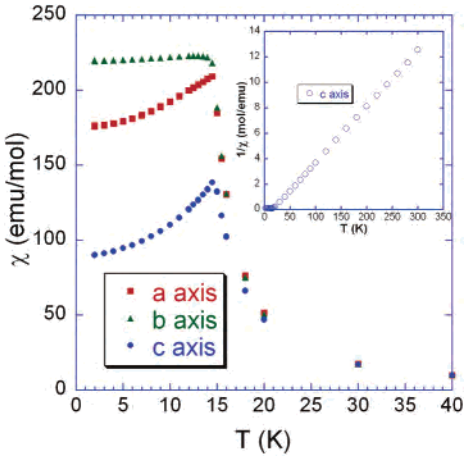

Figure 3. Susceptibility of $Eu_3In_2P_4$ as a function of temperature with 0.1 T applied field. The inset shows the $1/\chi$ vs T plot in the c axis orientation.

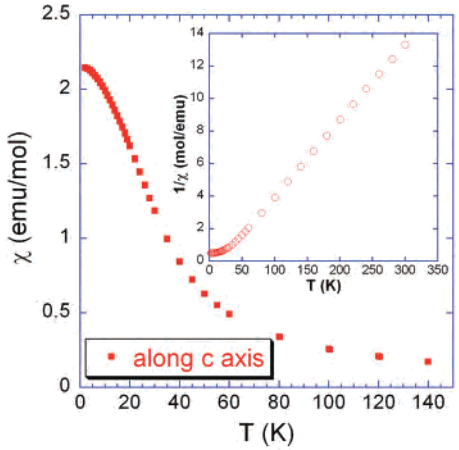

Figure 4. Susceptibility as a function of temperature with 5 T applied field. The data were measured with the applied field parallel to the crystal c axis. The inset shows the $1/\chi$ vs T plot.

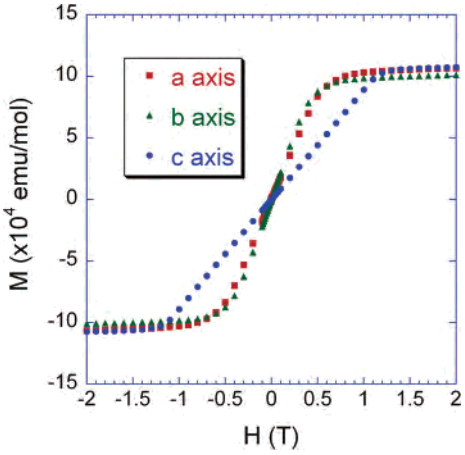

Figure 5. Magnetization of $Eu_3In_2P_4$ as a function of applied field at 5 K.

Eu−Eu distance in this compound, and it is close to the shortest Sr−Sr distance (3.665 Å) in $Sr_3In_2P_4$. The next shortest distance is much longer: 4.2712(9) Å between two adjacent Eu(1) (or adjacent Eu(2)) atoms along the c axis direction.

The structure of $Eu_3In_2P_4$ can be explained by the Zintl concept, as has been done for $Sr_3In_2P_4$ and $Ca_3In_2As_4$.[20] The charge of the anionic unit, $[In_2P_4]^{6-}$, can be balanced with divalent Eu atoms.

Magnetism. The temperature-dependent magnetic susceptibility between 2 and 40 K with 0.1 T applied field is shown in Figure 3. ZFC and FC data were identical in all three orientation measurements. At high temperatures, the curves of the different orientations are very similar, and they can be fit with the Curie−Weiss law

$$\chi = \frac{C}{T - \theta}$$

The result gives an average of $C = 22.65(5)$ emu K/mol and $\theta = 16.9(8)$ K. The C value corresponds to a total formula effective moment of 13.46(4) μ_B, close to the theoretical value of 13.75 μ_B for three $^8S_{7/2}$ Eu^{2+} cations. The $1/\chi$ vs T data, for the c axis orientation with an applied field of 0.1 T are shown in the inset to Figure 3.

In the low-temperature range there is an obvious magnetic transition at 14.5 K. There is a deviation from the magnetic susceptibility curve as a function of crystal anisotropy at temperatures as high as 30 K. This may arise from short-range ordering above the transition temperature. According to the shape of the susceptibility curves, antiferromagnetism is dominant at low temperatures. However, there are two anomalies with regard to normal antiferromagnetic (AFM) behavior: first, the susceptibility in the c axis direction is much smaller than in the other two directions; second, below 14.5 K, the susceptibility decreases with temperature in both the a and c axis direction. In addition, the positive Weiss constant suggests a ferromagnetic (FM) interaction at high temperatures, another deviation from traditional antiferromagnetism. This phenomenon has been observed in several Eu-containing intermetallic and Zintl phases such as $EuGa_4$, $EuMn_2P_2$, and EuSnP.[11,12,16] In those reports the authors suggested that there is a coexistent ferromagnetic ordering component that gives rise to this effect.[11,12,16]

The χ vs T data were obtained with an applied field of 5 T. The shape of the susceptibility curve is no longer reminiscent of antiferromagnetism. Instead, the susceptibility (Figure 4) monotonically increases with decreasing temperature as with a ferromagnet.

The magnetic hysteresis curves at 5 K also suggest antiferromagnetism. As shown in Figure 5, the magnetization increases linearly with the applied field in all the three orientations. The magnetization value saturates at about 1.6 T for the c axis and 1 T for the a and b axis. These are low saturation fields compared to typical antiferromagnets and suggest that the antiferromagnetic interaction is very weak. No spin-flop transition was observed for any crystal orientation up to 3 T. The saturation magnetization is approximately $1.070(6) \times 10^5$ emu/mol (19.23(2) μ_B per formula), which is slightly smaller than the value calculated from three Eu^{2+} ions per formula (21 μ_B). The hysteresis measurement provides insight into the χ vs T data, which show AF ordering at low fields (Figure 3) and FM ordering at high fields (Figure 4). The FM ordering occurs because

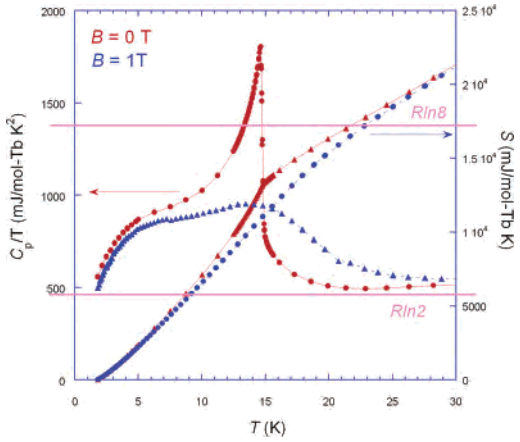

Figure 6. Heat capacity and entropy of $Eu_3In_2P_4$ in both 0 and 1 T field.

the high field saturates the sample and makes all the moments align in the same direction in a ferromagnetic fashion.

Heat Capacity. Figure 6 shows the result of heat capacity measurements. The data are shown in C_p/T, normalized to per mole of europium. There is a sharp peak at about 14.5 K in the zero-field measurement, which corresponds to the transition seen in the susceptibility measurement. The tail above 14.5 K is considered to be due to short-range magnetic ordering. Under an applied magnetic field of 1 T, this peak broadens and shifts to a higher temperature due to the saturation of the magnetic moment associated with the FM character of the spin. The entropy of R ln 8, which corresponds to the full three Eu^{2+} states, is reached at about 22 K, indicating that the system has an 8-fold degenerate Eu^{2+} ground state, as expected from susceptibility data. The broad increase between 3 and 8 K is very similar to that observed in Eu_3InP_3.[19] This broad increase in Eu_3InP_3 was explained as an intrinsic magnetic transition, since a peak was seen in susceptibility measurement at around 5 K.[19] However, there is no transition in the χ vs T plot of $Eu_3In_2P_4$ in this temperature range, suggesting it is not specifically due to the particular structure of Eu sites. Indeed, this kind of broad feature appears in several Eu^{2+} and Gd^{3+} systems, regardless of the crystal structures.[25−29] Below the transition temperature, there remains R ln 2 of entropy, which corresponds to R ln 8 for the three Eu cases. These facts together suggest that this broad feature is most likely due to the Zeeman splitting of the 8-fold degenerated states at the local Eu^{2+} site by internal magnetic field produced by magnetic ordering below the transition temperature. We expect the same physics in Eu_3InP_3 for the low-temperature feature around 5 K, that is, the increase in heat capacity at around 5 K in Eu_3InP_3 is not due to an intrinsic magnetic transition, and the peak in the χ vs T plot of Eu_3InP_3 at 5 K may be attributed from the local environment of spins.

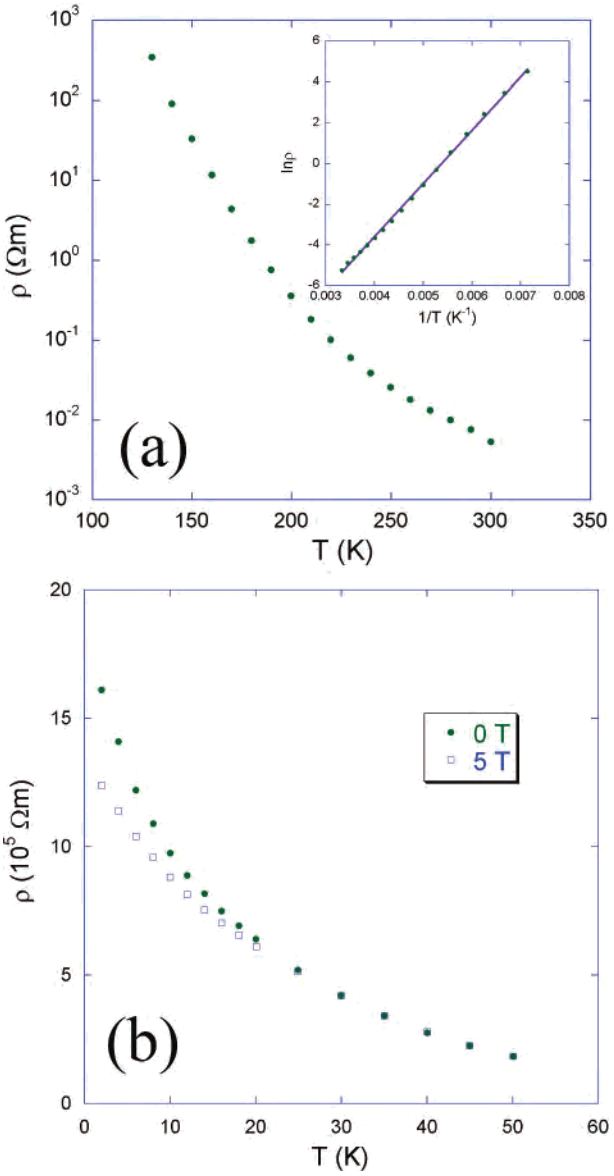

Figure 7. Charge-transport measurement. (a) Resistivity as a function of temperature. The inset shows ρ versus $1/T$ and the linear fit to the data. (b) Low-temperature resistivity as a function of temperature in 0 and 5 T applied magnetic field.

Resistivity. The temperature-dependent resistivity (ρ) data are shown in Figure 7. Figure 7a shows the high-temperature data measured with a four-lead method, and Figure 7b shows the low-temperature data measured with a two-lead method. The resistivity at room temperature is 0.005(1) Ω m. In the high-temperature region ln ρ as a function of inverse temperature can be linearly fit with the equation $\ln \rho = E_g/2k_BT + f$, which suggests that this compound is a semiconductor. The fitting of the data between 130 and 300 K provides the gap energy $E_g = 0.452(4)$ eV. Since this compound is a charge-balanced Zintl phase, its semiconducting property is expected according to the Zintl concept.

(25) Brown, S. E.; Thompson, J. D.; Willis, J. O.; Aikin, R. M.; Zirngiebl, E.; Smith, J. L.; Fisk, Z.; Schwarz, R. B. *Phys. Rev. B: Condens. Matter* **1987**, *36*, 2298−300.
(26) Thompson, J. D.; Cheong, S. W.; Brown, S. E.; Fisk, Z.; Oseroff, S. B.; Tovar, M.; Vier, D. C.; Schultz, S. *Phys. Rev. B: Condens. Matter* **1989**, *39*, 6660−6.
(27) Hossain, Z.; Trovarelli, O.; Geibel, C.; Steglich, F. *J. Alloys Compd.* **2001**, *323*−*324*, 396−399.
(28) Sullow, S.; Prasad, I.; Aronson, M. C.; Sarrao, J. L.; Fisk, Z.; Hristova, D.; Lacerda, A. H.; Hundley, M. F.; Vigliante, A.; Gibbs, D. *Phys. Rev. B: Condens. Matter* **1998**, *57*, 5860−5869.
(29) Canfield, P. C.; Thompson, J. D.; Beyermann, W. P.; Lacerda, A.; Hundley, M. F.; Peterson, E.; Fisk, Z.; Ott, H. R. *J. Appl. Phys.* **1991**, *70*, 5800−2.

Magnetoresistance at high temperatures is nonobservable. While at low temperatures, as shown in Figure 7b, the magnetoresistance onset occurs below approximately 30 K. This temperature is coherent with the temperature at which the magnetic anisotropy becomes noticeable. The maximum magnetoresistance is about −30% at 2 K with an applied field of 5 T. AFM materials with magnetoresistance are very rare, and very often these types of materials are metallic.[30−32] If this compound is antiferromagnetic, and the applied field is parallel to the spin moment direction (*c* axis), the magnetoresistance should be positive according to theory.[33] But here a negative magnetoresistance is observed in a field as high as 5 T, the spin moments in the compound are saturated in the field direction, and the compound is in an induced ferromagnetic configuration. This transition could cause a "red-shift effect" similar to that of EuSe,[34] which can lower the resistivity. Also, in the ferromagnetic state, the current carriers (electrons) can avoid scattering when hopping from site to site, because all sites have the same spin moment direction. This can also decrease the resistivity.

Since this compound is a semiconductor, the interaction should be the Bloembergen−Rowland (BR) coupling.[35] That is, interband exchange produces the magnetic interaction between Eu sites: phosphorus p electrons excited to the Eu d band and polarized by intraband f−d exchange. Alternatively, superexchange may occur between the two shortest Eu−Eu distances of 3.7401(6) and 4.2712(9) Å. A recent theoretical calculation suggests that Eu f shell superexchange interaction can produce a sizable effect in compounds with similar Eu−Eu distances.[36] These two possible mechanisms can compete between neighboring europium atoms and thus cause the weak, easily saturated, low-temperature antiferromagnetism in this compound. The positive Weiss constant in this compound is controversial. However, if we consider the structure, it is still understandable. The distances within one Eu triplet and between these triplets are very different, which means that the coupling within and between these triplets is different. There could be different types of couplings (one FM, the other AFM). If this is the case, a possible model might be with FM interactions within triplets and AFM interactions between triplets. With this model, the FM ordering would be short range and could be reflected in the Weiss constant, while the AFM ordering could be long range at low temperatures. This model provides one way to explain all the data. We plan to use neutron diffraction to determine the magnetic structure, and efforts are underway to grow large crystals for this experiment.

Summary. $Eu_3In_2P_4$ is a magnetic semiconducting compound with a transition temperature at 14.5 K. While there are aspects of the temperature dependence of the magnetic data that suggest weak antiferromagnetic order, there are also components that suggest ferromagnetism. Its magnetic property is anisotropic, and the Weiss constant θ is positive. Heat capacity shows a magnetic transition that is suppressed with field, consistent with AF at low field and FM at high field. At the magnetic ordering temperature, this compound shows a negative magnetoresistance. There are two crystallographically different Eu^{2+} sites in this compound. We have proposed a simple model relating structure to the magnetic properties. Further efforts are under way to investigate this model with neutron diffraction.

Acknowledgment. The authors thank Prof. Kai Liu for discussion. We acknowledge funding by the NSF (DMR-0120990). The work in the Physics Department was supported by NSF DMR-0433560.

Supporting Information Available: Crystallographic data is provided in CIF format. This material is available free of charge via the Internet at http://pubs.acs.org.

IC0504036

(30) Das, I.; Sampathkumaran, E. V. *Phys. Rev. B: Condens. Matter* **1994**, *49*, 3972−4.
(31) Sampathkumaran, E. V.; Das, I. *Phys. Rev. B: Condens. Matter* **1995**, *51*, 8631−3.
(32) Chan, J. Y.; Kauzlarich, S. M.; Klavins, P.; Shelton, R. N.; Webb, D. J. *Phys. Rev. B: Condens. Matter* **1998**, *57*, R8103−R8106.
(33) Yamada, H.; Takada, S. *J. Phys. Soc. Jpn.* **1973**, *34*, 51−7.
(34) Wachter, P. Europium Chalcogenides: EuO, EuS, EuSe and EuTe. In *Handbook of Physics and Chemistry of Rare Earths*, Gschneidner, K. A. J., Eyring, L. R., Eds.; North-Holland: Amsterdam, 1979; Vol. 2, pp 507−574.
(35) Lee, V. C.; Liu, L. *Phys. Rev. B: Condens. Matter* **1984**, *30*, 2026−35.
(36) Kunes, J.; Ku, W.; Pickett, W. E. Exchange coupling in Eu monochalcogenides from first principles. In *Los Alamos National Laboratory, Preprint Archive, Condensed Matter*, 2004; pp 1−4, arXiv: cond-mat/0406229.